Anal. Chem. **2002,** *74,* 6170−6176

Nanochannels on a Fused-Silica Microchip and Liquid Properties Investigation by Time-Resolved Fluorescence Measurements

Akihide Hibara,[†] Takumi Saito,[†] Haeng-Boo Kim,[†] Manabu Tokeshi,[‡] Takeshi Ooi,[§] Masayuki Nakao,[§] and Takehiko Kitamori*[,†,‡,∥]

Department of Applied Chemistry, School of Engineering, The University of Tokyo, 7-3-1 Hongo, Bunkyo-ku, Tokyo 113-8656, Japan, Integrated Chemistry Project, Kanagawa Academy of Science and Technology, 3-2-1 Sakado, Takatsu-ku, Kawasaki-shi, Kanagawa 213-0012, Japan, Department of Engineering Synthesis, School of Engineering, The University of Tokyo, 7-3-1 Hongo, Bunkyo-ku, Tokyo 113-8656, Japan, and Precursory Research for Embryonic Science and Technology, Japan Science and Technology Corporation

We have fabricated nanometer-sized channels, demonstrated a technique for the introduction of liquid into the channels, and carried out time-resolved fluorescence measurements of aqueous solutions. In this study, 330-nm- and 850-nm-sized channels were fabricated on fused-silica substrates by fast atom beam etching and hydrofluoric acid bonding methods. A liquid introduction method utilizing capillary action was demonstrated. The liquid introduction was observed under an optical microscope, and the liquid velocity during the introduction was analyzed by surface energy and macroscale hydrodynamics. The liquid velocity due to capillary action in the nanometer-sized channel seemed more than four times slower than the estimation. Then, aqueous solutions of rhodamine 6G (R6G), sulforhodamine 101 (SR101), and rhodamine B (RB) in the channels were measured by time-resolved fluorescence spectroscopy; spectra of the same solution in a 250-μm-sized channel were also measured as a reference for the macrospace. Although the fluorescence spectra in the 330-nm-, 850-nm- and 250-μm-sized channels agreed with one another, the fluorescent decays in the nanometer-sized channels were faster for R6G and SR101 and slower for RB than the respective decays in the 250-μm-sized channels. The results suggested the solutions had lower dielectric constants and higher viscosities in the nanometer-sized channels.

Microchip technology has been investigated mainly by analytical chemists and engineers of microelectromechanical systems (MEMS) because it has numerous desirable features, such as high throughput, space and labor savings, high reproducibility, and small sample requirements.[1−3] One of the most important investigation fields has been integration of flow chemical processing,[4−10] from which investigations considerably complex chemical systems have been realized. In particular, the concepts of the continuous flow chemical processing (CFCP) and microunit operations (MUO)[5] are expected to advance integration density of microchip chemistry in a way similar to the advances in electronics from IC to ULSI. Smaller and thinner channels in nanometer (submicrometer) scale are natural consequences. Important and complex problems concerning the nanometer-sized channels are how hydrodynamic properties and collective behaviors of a liquid change as compared with the bulk liquid. Investigations into mesoscopic liquids allow informative discussions on the basic science of liquids and solutions.

Since the specific interface area of the channel becomes higher on miniaturizing the channel width, interfacial phenomena, such as surface charge of substrates and surface traps, may affect the analysis.[11] Space-confinement phenomena have been investigated in nanometer-sized pores of synthetic and natural nanomaterials.[12] However, the intermediate submicrometer-sized space between the nanomaterial and the fabricated micrometer-sized channel has not been investigated because of a lack of experimental methods. Channels of this scale are interesting from two viewpoints, engineering and basic chemistry. From the engineering viewpoint, the submicrometer-sized channel is regarded as the lower limit of channel size. It should be investigated from which depth and width a liquid can no longer be regarded as an ordinary fluid. From the basic chemistry viewpoint, it should be investigated what

* To whom correspondence should be addressed. Fax: +81-3-5841-6039. E-mail: kitamori@icl.t.u-tokyo.ac.jp.

[†] Department of Applied Chemistry, The University of Tokyo.

[‡] Kanagawa Academy of Science and Technology.

[§] Department of Engineering Synthesis, The University of Tokyo.

[∥] Japan Science and Technology Corporation.

(1) *Proceedings of Micro Total Analysis Systems 2001*; Ramsey, J. M., van den Berg, A., Eds.; Kluwer Academic Publishers: Dordrecht, 2001.

(2) Manz, A.; Graber, N.; Widmer, H. M. *Sens. Actuators, B* **1990**, *1*, 244−248.

(3) Harrison, D. J.; Fluri, K.; Seiler, K.; Fan, Z. H.; Effenhauser, C. S.; Manz, A. *Science* **1993**, *261*, 895−897.

(4) Hibara, A.; Tokeshi, M.; Uchiyama, K.; Hisamoto, H.; Kitamori, T. *Anal. Sci.* **2001**, *17*, 89−93.

(5) Tokeshi, M.; Minagawa, T.; Uchiyama, K.; Hibara, A.; Sato, K.; Hisamoto, H.; Kitamori, T. *Anal. Chem.* **2002**, *74*, 1565−1571.

(6) Weigl, B. H.; Yager, P. *Science* **1999**, *283*, 346−347.

(7) Kopp, M. U.; de Mello, A. J.; Manz, A. *Science* **1998**, *280*, 1046−1048.

(8) Lagally, E. T.; Medintz, I.; Mathies, R. A. *Anal. Chem.* **2001**, *73*, 565−570.

(9) Kenis, P. J. A.; Ismagilov, R. F.; Whitesides G. M. *Science* **1999**, *285*, 83−85.

(10) Beebe, D. J.; Moore, J. S.; Yu, Q.; Liu, R. H.; Kraft, M. L.; Jo, B. H.; Devadoss, C. *Proc. Nat. Acad. Sci.* **2000**, *97*, 13488−13493.

(11) Xu, X.-H. N.; Yeung, E. S. *Science* **1998**, *281*, 1650−1653.

(12) For example, see Kageyama, K.; Tamazawa, J.; Aida, T. *Science* **1999**, *285*, 2113-2115.

10.1021/ac025808b CCC: $22.00
Published on Web 11/08/2002

determines the limitation of the channel size and how the channel size affects collective behaviors of molecules in a nanoscale confined environment. Furthermore, from a third viewpoint of fabrication and liquid handling techniques, we have developed a fabrication method for the smallest confined channel structure on fused-silica substrates by utilizing a fast atom beam method[13] and derived a liquid introduction method based on capillary action.[14] In this fabrication, the channel layout can be freely designed, and even complicated chemical operations[5] can be integrated to nanometer-sized channels. For realization of high integration density of chemical systems, the fabricated nanometer-sized channel has greater potential than thermal-drawing nanometer-sized capillary[15−17] and nanometer-deep micrometer-sized channels.[18,19] Furthermore, since the channel surface can be modified by various kinds of silane coupling reagents, we can control the surface properties of the channel when we study the size effect on liquids.

In this paper, we used a fast atom beam method to fabricate two-types of the nanometer-sized channels having widths of 330 and 850 nm. Liquid introduction utilizing capillary action was observed, and the liquid velocity was analyzed by macroscale hydrodynamics. Furthermore, liquid properties in the channels were studied based on time-resolved fluorescent spectroscopy of aqueous solutions of rhodamine dyes as probing molecules for viscosity, dielectric constant, and surface adsorption. We discuss in terms of adsorption of the dyes onto the channel surface, viscosity of aqueous solution, dielectric property of confined liquid, and optical cavity effects.

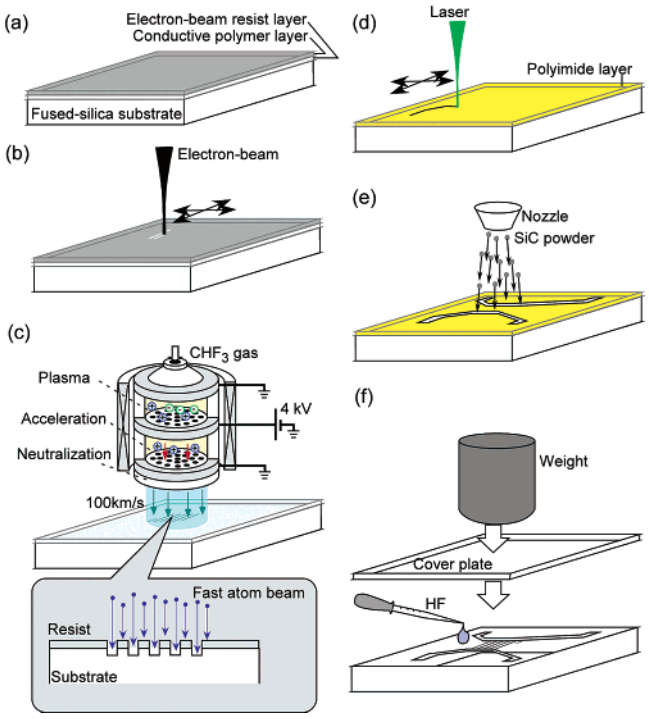

Figure 1. Fabrication scheme: (a) spin coating of electron-beam resist and conductive polymer layers on fused-silica substrate, (b) electron-beam lithography of nanometer-sized channels, (c) fast atom beam etching of nanometer-sized channels, (d) laser patterning of micrometer-sized channels, (e) sand-blast processing of micrometer-sized channels, and (f) hydrofluoric acid bonding of the cover plate.

EXPERIMENTAL SECTION

Electron Beam Lithography. The fabrication scheme is shown in Figure 1. Substrates were 1-mm-thick fused-silica rectangle plates with 35- and 70-mm sides. The substrates were mechanically polished and thermally annealed to obtain an optically flat surface. The substrates were successively washed in acetone, ethanol, and pure water and cleaned in an O_2-plasma reactor. First, the substrate was covered with electron-beam resist and conductive polymer layers by using a spin coater (Figure 1a). Then it was placed in the vacuum chamber of an electron-beam lithography system. A computer-controlled electron-beam scanner was used to draw a nanometer-sized channel pattern (Figure 1b). After the exposure, the conductive polymer layer was removed in pure water, and the electron-beam resist layer was developed in xylene.

Nanofabrication. Since conventional fabrication methods utilize accelerated charged particles for the etching source, it is difficult to use an insulating material, such as glass, as a result of the surface charge-up effect. Therefore, we used a fast atom beam fabrication method because it utilizes accelerated neutral particles, and the surface charge effect is negligible.[20,21] The method provided submicrometer-sized channels with high aspect ratios. The substrate was placed in a fast atom beam (FAB) fabrication chamber (Figure 1c). The FAB was obtained by ionization of CHF_3, acceleration of the ions by a high voltage, and neutralization. The fabrication depth was controlled using the beam irradiation time. After FAB etching, the resist layer was removed in the O_2 plasma chamber.

Microfabrication. To introduce liquid samples into the nanometer-sized channels, we also fabricated micrometer-sized channels on the substrate. Since an additional wet process may damage the nanometer-sized channel, micrometer-sized channels were fabricated by laser-beam patterning and sand-blast processing. First, the substrate was covered with a polyimide sheet and the micrometer-sized channel layout was patterned on the sheet by fourth harmonics of YAG laser (Figure 1d). Then, SiC powder (diameter, 12 μm) was applied to the substrate (Figure 1e). After the sand blast processing, the polyimide layer was removed. At each end of the channel, a 0.4-mm-diameter hole was drilled.

Cover Plate Bonding. To cover the nanometer- and micrometer-sized channels, a 170-μm-thick fused-silica plate was bonded to the substrate. In previous reports,[22,23] the fused-silica plates were

(13) Fujinami, M.; Tokeshi, M.; Odake, T.; Kitamori, T.; Sato, K.; Sawada, T.; Matsumoto, K.; Nakao, M.; Ooi, T.; Hatamura, Y. *Proc. Micro Total Anal. Syst. '98*, **1998**, 339−342.
(14) Hibara, A.; Saito, T.; Kim, H. B.; Tokeshi, M.; Ooi, T.; Nakao, M.; Kitamori, T. *Proc. 15th International Symposium on Microscale Separations and Analysis (HPCE2002)* 2002, 159.
(15) Lyon, W. A.; Nie, S. *Anal. Chem.* **1997**, *69*, 3400−3405.
(16) Zander, C.; Drexhage, K. H.; Han, K. T.; Wolfrum, J.; Sauer, M. *Chem. Phys. Lett.* **1998**, *286*, 457−465.
(17) Woods, L. A.; Roddy, T. P.; Paxon, T. L.; Ewing, A. G. *Anal. Chem.* **2001**, *73*, 3687−3690.
(18) Jacobson, S. C.; Alarie, J. P.; Ramsey, J. M. *Proc. Micro Total Anal. Syst. 2001* **2001**, 57−59.
(19) Clicq, D.; Vervoort, N.; Baron, G. V.; Desmet, G. *Proc. 15th International Symposium on Microscale Separations and Analysis (HPCE2002)* 2002, 56.
(20) Hatakeyama, M.; Tanaka, S.; Ichiki, K.; Toma, Y.; Nakao, M.; Hatamura, Y. *Microsyst. Technol.* **1997**, *3*, 112−116.
(21) Ichiki, K.; Hatakeyama, M.; Tanaka, S.; Nakao, M.; Hatamura, Y. *Thin Solid Films* **1996**, *281−282*, 630−633.
(22) Sato, K.; Kawanishi, H.; Tokeshi, M.; Kitamori, T.; Sawada, T. *Anal. Sci.* **1999**, *15*, 525−529.

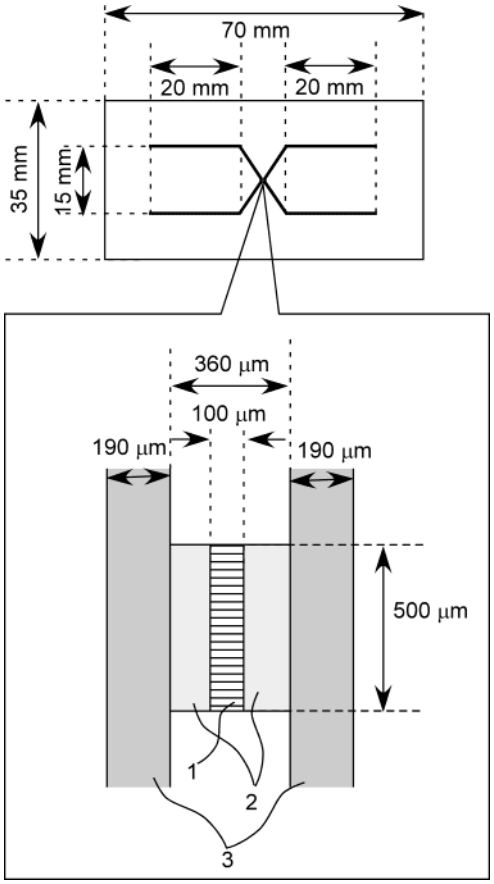

Figure 2. Layout of channels. The 190-μm-wide channels are designed for pressure-driven liquid introduction. The lower sketch shows an expanded view around the nanometer-sized channels. Area 1 is a 100 $\times$ 500 μm fabrication area of the nanometer-sized channels, and 250 parallel channels are fabricated in the horizontal direction of the figure. Area 2 is the connection channel area between the nanometer- and micrometer-sized channels. Area 3 is the liquid introduction channel area.

laminated by a thermal bonding method at the softening point of fused silica (1150 °C). Since softening of glass may deform the nanometer-sized channel beyond use, we chose a hydrofluoric acid bonding method at room temperature. Next, the substrates were laminated with the 170-μm-thick fused-silica plate by a hydrofluoric acid bonding method at room temperature.[24] The substrate and cover plates were successively washed in acetone, ethanol, pure water, a mixed solution of sulfuric acid and hydrogen peroxide (2:1), 1 M NaOH solution, and pure water. Then, 1% HF solution was dropped between the substrate and cover plates and the plates were pressed with a 12-kg weight for 24 h (Figure 1f). Completeness of the bonding was confirmed by sight and a leakage test observed under an optical microscope. If the bonding had failed, an optical interference ring pattern was observed.

Channel Layout. The design of the nanometer- and micrometer-sized channels is shown in Figure 2. The nanometer-sized channels (area 1, 100 $\times$ 500 μm) were fabricated between two 190-μm-wide channels (area 3). The nanometer-sized channels and 190-μm-wide channels were connected by 500-μm-wide shallow

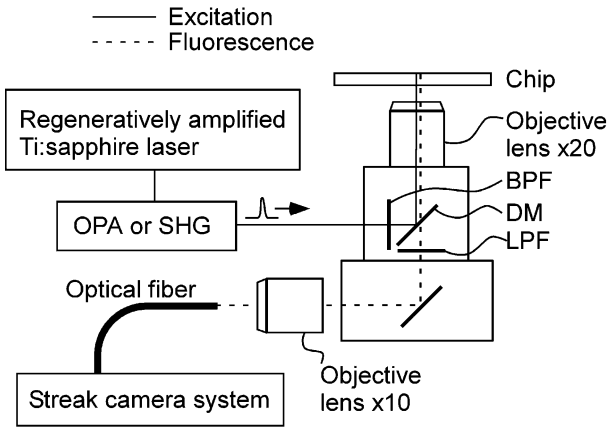

Figure 3. Schematic diagram of the time-resolved fluorescence measurement system.

channels (area 2) having the same depth as the nanometer-sized channels. Areas 1 and 2 were fabricated by the FAB method, and area 3 was fabricated by sand-blast processing. In area 1, 250 parallel channels were fabricated along the horizontal direction with a period of 2 μm.

Liquid Introduction. The fused-silica chip was sandwiched with aluminum holders in order to connect glass capillary tubes to the channels through the holes. Sample solutions and other flushing solvents were introduced by a syringe pump connected to the capillary tubes. Details about the holders and connections were reported previously.[25] Aqueous solutions of rhodamine 6G (R6G), sulforhodamine 101 (SR101), and rhodamine B (RB) were used as samples. The flushing process was also observed with fluorescence measurements, where decrease of fluorescence was confirmed with repetition of flushing.

Time-Resolved Measurement. A schematic diagram of time-resolved fluorescence measurement system is shown in Figure 3. A Ti−sapphire laser having a wavelength of 800 nm, a temporal duration of 50 fs, and repetition rate of 100 kHz was used as the excitation light source. By using an optical parametric amplifier (OPA) or second harmonic generation (SHG) crystal, we converted the wavelength of the laser pulse to 400 nm (R6G) or 532 nm (SR101 and RB). After passing through a band-pass filter (BPF) and reflecting on a dichroic mirror (DM), the excitation pulse was focused onto the channels through a $\times$20 objective lens (N.A., 0.75). The transmit/reflect switching wavelength of DM was 420 (R6G) or 565 nm (RB, SR101). The intensity of the excitation pulse under the objective lens was reduced to 100 μW (1 nJ/pulse). Fluorescence was collected by the same objective lens and transmitted DM and a long pass filter (LPF). The LPF threshold was 560 (RB, SR101) or 420 nm (R6G). The fluorescence was introduced to an optical fiber through a $\times$10 objective lens (N.A., 0.30). The spectrum and decay curve were simultaneously analyzed by a streak camera system.

RESULTS AND DISCUSSION

Fabrication and Liquid Introduction. Before laminating the cover plate, the fabrication depth and the channel width were measured. To measure the fabrication depth, the depth of the connection area was measured by a contact profilometer along

(23) Sato, K.; Tokeshi, M.; Kitamori, T.; Sawada, T. *Anal. Sci.* **1999**, *15*, 641−645.
(24) Nishimoto, T.; Nakanishi, H.; Abe, H.; Arai, A.; Nakamura, R.; Yotsumoto, A.; Shoji, S. *Proc. Micro Total Anal. Syst. '98*, **1998**, 311−314.
(25) Tokeshi, M.; Minagawa, T.; Kitamori, T. *Anal. Chem* **2000**, *72*, 1711−1714.

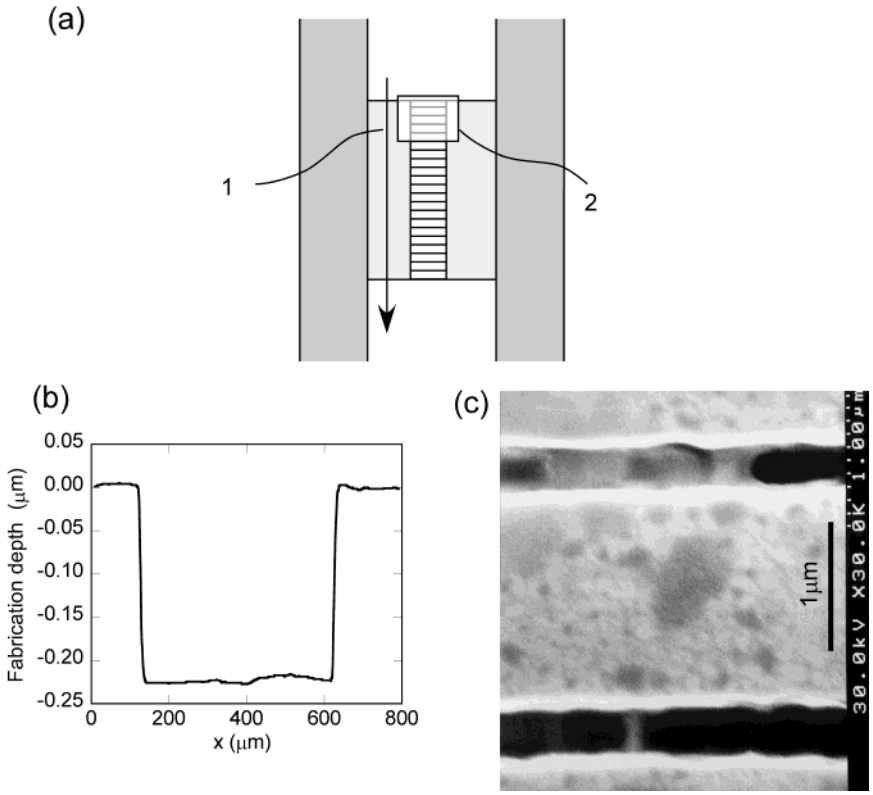

Figure 4. (a) Illustration of the area around the nanometer-sized channels; 1 and 2 indicate scanning line of fabrication depth measurement and optical microscope observation area of liquid introduction; (b) fabrication depth measurement results obtained by a contact profilometer; and (c) SEM image of the nanometer-sized channels.

line 1 in Figure 4a. Figure 4b shows the fabrication depth measurement results. By averaging the fabrication depth between 200 and 600 μm, the fabrication depth was determined to be 220 nm. The channel width was measured from SEM images. Figure 4c shows the SEM image of the fabricated nanometer-sized channels, where the conductive polymer layer was spin-coated. The white and black areas correspond to nonfabricated and fabricated areas, respectively. By measuring the width of the black area, the channel width was determined to be 330 nm. Then, the width and depth of the fabricated nanometer-sized channel were determined to be 330 and 220 nm (330-nm channel), respectively. We also fabricated another nanometer-sized channel having a 850-nm width and 650-nm depth (850-nm channel).

To get liquid introduction without any air bubbles, we applied a capillary action method. The liquid mechanical properties in the nanometer-sized channel can be investigated by measuring liquid introduction behavior. Figure 5 shows the results of optical microscope observation of water introduction to the 330-nm channel by a high-speed camera (500 frame/s). Figure 5a illustrates the image during the water introduction process. The front line of water can be observed as the border between water-filled and vacant channels. Figure 5b corresponds to the image just before water introduction, and Figure 5c−e corresponds to those after 4, 8, and 12 ms, respectively. When air in the channel was replaced by water, contrast of the images was reduced, because the difference in refractive indices between the fused silica ($n = 1.45$) and the vacant channel ($n = 1.00$) was matched by filling the channel with water ($n = 1.33$). The air bubble in the channel was completely replaced by water within 1 s. The front line of water traveled along the 100-μm-long channel during five frames (10 ms). Therefore, the linear flow rate was estimated as 10 mm/s. In this case, the driving force was surface energy (Laplace pressure, ΔP), expressed as

$$\Delta P = \frac{2\gamma}{r} \tag{1}$$

where γ and r represent surface tension and the radius of curvature, respectively. When 132 nm (half of hydrodynamic diameter, $D = 264$ nm) was used as r, ΔP was estimated as 1.0 MPa. When macroscale fluid dynamics is assumed, pressure drop ΔP_d can be expressed as[26,27]

$$\Delta P_d = \frac{32\mu v L}{D^2} \tag{2}$$

where μ and v are viscosity and velocity of fluid. L is the distance between two points where ΔP_d is considered. Although the pressure drop ΔP_d should be smaller than the Laplace pressure ΔP in the introduction process, we assumed $\Delta P_d = \Delta P$ in order to estimate theoretical introduction time, $\langle t \rangle$, and mean velocity,

(26) Bird, R. B.; Stewart, W. E.; Lightfoot, E. N. *Transport Phenomena*; John Wiley & Sons: New York, 1960; Chapter 6.
(27) Hibara, A.; Nonaka, M.; Hisamoto, H.; Uchiyama, K.; Kikunani, Y.; Tokeshi, M.; Kitamori, T. *Anal. Chem.* **2002**, *74*, 1724−1728.

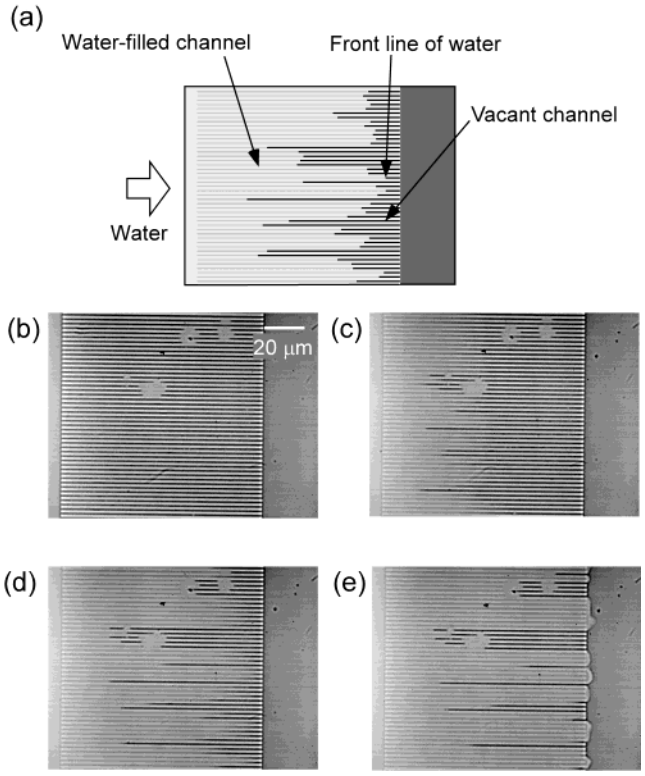

Figure 5. (a) Illustration of water introduction process into the nanometer-sized channels under an optical microscope. The water-filled channels were observed with lower contrast than the vacant channels. (b)−(e) Optical microscope images of the 330-nm-sized channels during water introduction. The images were measured (b) just before water introduction (0 ms), after (c) 4, (d) 8, and (e) 12 ms. The images were recorded at 500 frames/s (2 ms period), and the shutter speed was 2 ms.

$\langle v \rangle$. In the case of channel length L', $\langle t \rangle$ can be formulized as

$$\langle t \rangle = \int_0^{L'} \frac{\mathrm{d}L}{v} = \int_0^{L'} \frac{32\mu L}{D^2 \Delta P} \mathrm{d}L = \frac{16\mu L'^2}{D^2 \Delta P} \quad (3)$$

In our case, the channel length L' is 100 μm. On the basis of these assumptions, the introduction time $\langle t \rangle$ and mean velocity $\langle v \rangle$ ($= L'/\langle t \rangle$) were estimated as 2.3 ms and 43 mm/s, respectively. The analysis suggested that the liquid velocity in the 330-nm channel was more than four times slower than the estimation. As long as macroscale dynamics was assumed, the slower velocity suggested higher viscosity in the 330-nm channels.

Since the width and depth of the nanometer-sized channels are smaller than or comparable to the diffraction limit of visible light, it has been difficult to analyze flow properties exactly in the nanometer-sized channels. Although the temporal resolution of the present analysis was not enough for a strict discussion, our method combining imaging of the liquid introduction process and hydrodynamic analysis should be important for development of nanofluidics.

Spectroscopic Measurements. To compare the fluorescence responses in normal bulk-scale liquid with those in the nanometer-sized channels, a microchannel having 250-μm width and 100-μm depth (250-μm channel) was used as a reference. The electronic states and solvent effects were investigated by measuring spectral shapes and the temporal response of fluorescent decay. One distinct feature of the nanometer-sized channels is high specific interface area, which is defined as the interface area-to-volume ratio. The specific interface areas of the 250-μm, 850-nm, and 330-nm channels are 0.028 μm^{-1}, 5.4 μm^{-1}, and 15 μm^{-1}, respectively. In the case of a cylindrical tube having a diameter of 1 cm, the specific interface area is 0.0004 μm^{-1}. Since the specific interface area in the nanometer-sized channel is much higher than those in bulk tubes, adsorption phenomena may be emphasized, and surface charge and surface functional groups may affect liquid properties, such as viscosity. In this report, the fused-silica surface was not coated with an additional group, and therefore, the surface was negatively charged because of the silanol group in aqueous solution around pH of 7.

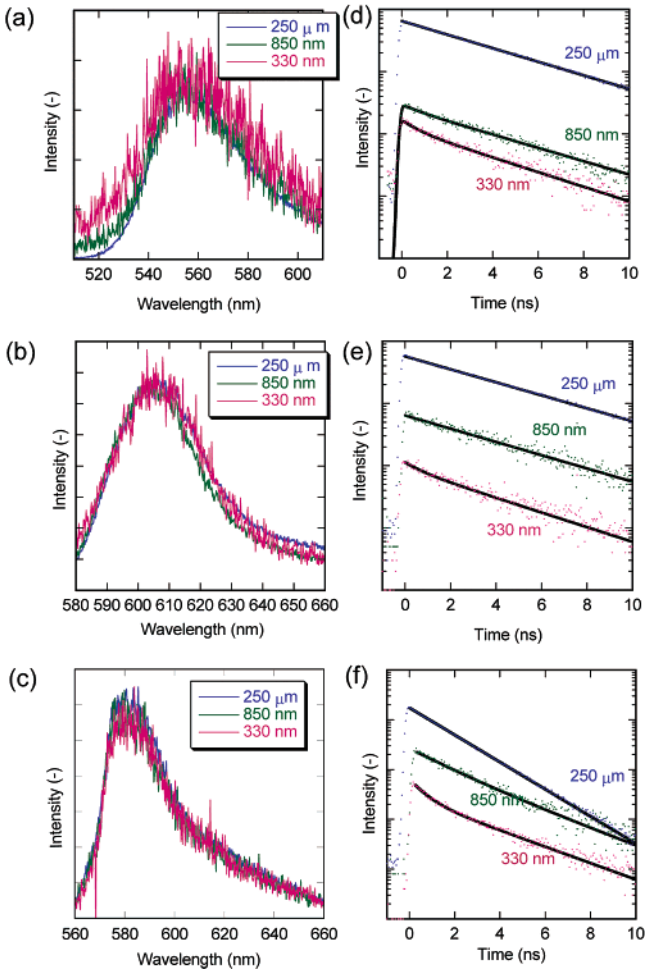

Figure 6. Fluorescence spectra of (a) R6G, (b) SR101, and (c) RB. Decay curves of (d) R6G, (e) SR101, and (f) RB. The spectra and decay curves were measured for the 250-μm, 850-nm, and 330-nm channels. The solid lines in the decay curves are fitted results obtained by a single or biexponential function. The fitted parameters are shown in Table 1.

Figure 6 shows typical results of the fluorescence measurements. Figures 6a−c show the fluorescence spectra of 1μM R6G, 1μM SR101 and 1μM RB, respectively. As shown in the figures, the fluorescence spectra agreed with one another within the experimental errors. Since spectra of these dyes absorbing on

Table 1. Fitted Results of Time-Resolved Fluorescence Measurements

dye	size	concn, μM	τ_1 (ns)	τ_2 (ns)	A_1	A_2
R6G	250 μm	1	3.98		1.00	
		10	4.03		1.00	
		100	4.02		1.00	
	850 nm	1	4.00	0.65	0.85	0.15
		10	3.64	0.38	0.90	0.10
		100	3.66	0.39	0.86	0.14
	330 nm	1	3.64	0.64	0.69	0.31
		10	3.01	0.50	0.60	0.40
		100	2.82	0.15	0.20	0.80
SR101	250 μm	1	4.16		1.00	
		10	4.19		1.00	
		100	4.17		1.00	
	850 nm	1	4.08		1.00	
		10	4.07		1.00	
		100	4.11		1.00	
	330 nm	1	3.35	0.73	0.79	0.21
		10	3.42	0.48	0.83	0.17
		100	3.71	0.47	0.86	0.14
RB	250 μm	1	1.59		1.00	
		10	1.58		1.00	
		100	1.59		1.00	
	850 nm	1	2.56	1.43	0.57	0.43
		10	2.50	1.28	0.47	0.53
		100	2.46	1.42	0.23	0.77
	330 nm	1	2.64	0.60	0.50	0.50
		10	2.57	0.70	0.55	0.45
		100	2.49	1.08	0.45	0.55

silica should change significantly,[28] fluorescence from the liquid phase was the dominant component in our spectral measurements. In addition, the results meant that the structure of the energy levels at ground and excited states of the probe molecules were not affected by the size of the channels.

Figures 6d−f show the fluorescence decay curves of 1 μM R6G, SR101, and RB, respectively. The decay times and waveforms apparently depended on the size of the channels, especially for RB. For the decay process analysis, a biexponential function was assumed for the decay curves as

$$S(t) = A_1 \exp\left(-\frac{t}{\tau_1}\right) + A_2 \exp\left(-\frac{t}{\tau_2}\right) \qquad (4)$$

where A_1 and A_2 are preexponential factors and τ_1 and τ_2 are decay times. The solid lines in Figures 6d−f indicate the fitting results of eq 4. To discuss the adsorption effect, 10 μM and 100 μM solutions of all dyes were also measured. The fitted results are summarized in Table 1. The sum of A_1 and A_2 was normalized to unity. When the difference between τ_1 and τ_2 was not significant, fitted results by a single-exponential model were adopted.

First, we compared R6G and SR101 in order to discuss the size effect and adsorption. R6G and SR101 have a fluorescent quantum yield close to unity, and the size effect due to a change in the dielectric constant may be estimated.[29] Since the ethylamino group gives R6G a positive charge, it easily adsorbs onto the negatively charged fused-silica surface. On the other hand, SR101 has both positively charged amino and negatively charged sulfonic groups, and therefore, adsorption of SR101 may be suppressed. In Table 1, R6G in the 250-μm channel and SR101 in the 250-μm and 850-nm channels could be fitted with the single-exponential model, and their decay times were close to the literature values of 4.08 (R6G)[29] and 4.12 ns (SR101).[30] For R6G in 850- and 330-nm channels and for SR101 in 330-nm channels, the decay curve should be fitted with the biexponential function. The preexponential factor for the faster component A_2 increased with a decrease in the size, which meant higher specific interface area, and the faster component of R6G appeared in the lower specific interface area than that of SR101. Therefore, we concluded that the faster component corresponded to emission from adsorbed dyes. Furthermore, the slower component also became smaller compared with the bulk solution.

One possible explanation for the smaller decay times of the absorbing dyes is the microcavity effect, which has been observed in micrometer-sized liquid droplets.[31] In the microcavity effect, the spontaneous emission rate is modified, depending on the mode density of the microcavity.[31,32] Since the nanometer-sized channel fabricated in this study had a one-dimensional free boundary and two-dimensional confinement and comparable scale as the emission wavelength, the theory for microdroplets could not be applied as it is. Although an analysis based on the microcavity effect can be informative, we focused instead on the decay time changes in the slower component here. Since the slower component corresponded to emission from the liquid phase in the nanometer-sized channels, the decay time change may be assigned to changes in a solvent property. As reported in ref 29, the decay time of R6G becomes faster as the dielectric constant decreases; while the mechanism has not been clarified, a simple emission rate modulation due to dielectric constant change was suggested. If we assumed this explanation, the smaller decay time of the slower component could be interpreted as showing a lower dielectric constant in the nanometer-sized channels. In the nanometer-sized channels, we anticipated that a hydrogen-bond network would be well-developed due to the effect of the charged silanol group. As a result, dielectric polarization of the aqueous solution may be suppressed.

Next, we considered the results of RB. Since RB has diethylamino and carboxyl groups, RB has a cationic or zwitterion form in neutral solution. As shown in Table 1, RB in the 250-μm channel could be fitted with the single-exponential model, and the decay time was close to the literature value of 1.58 ns.[33] For RB in 850- and 330-nm channels, the decay curve should be fitted with the biexponential function. Since RB was in an equilibrium of cationic and zwitterion forms and the cations could be adsorbed onto the fused-silica surface easily, some part of the RB was adsorbed onto the surface. On the basis of the same consideration made for R6G and SR101, we concluded that the faster component corresponded to emission from adsorbed dye. Here, we also focused on the slower component of the emission from the liquid phase.

(28) Vieira Ferreira, L. F.; Lemos, M. J.; Reis, M. J.; Bottelho do Rego, A. M. *Langumuir* **2000**, *16*, 5673−5680.

(29) Magde, D.; Rojas, G. E.; Seybold, P. G. *Photochem. Photobiol.* **1999**, *70*, 734−744.

(30) Ishizaka, S.; Habuchi, S.; Kim, H. B.; Kitamura, N. *Anal. Chem* **2000**, *71*, 3382−3389.

(31) Barnes, M. D.; Kung, C. Y.; Whitten, W. B.; Ramsey, J. M. *Phys. Rev. Lett.* **1996**, *76*, 3931−3934.

(32) Yokoyama, H.; Brorson, S. D. *J. Appl. Phys.* **1989**, *66*, 4801−4805.

(33) López Arbeloa, F.; López Arbeloa, T.; Tapia Estévez, M. J.; López Arbeloa, I. *J. Phys. Chem.* **1991**, *95*, 2203−2208.

The decay times of the slower component of RB became larger with the decrease of the channel size, which was in the direction opposite to the size dependence of R6G and SR101. Photophysical properties of RB are complicated compared with those of R6G or SR101, and some mechanisms have been proposed for solvent-dependent decay time.[29,33,34] In the simplest model, the excitation energy deactivates through tortional motion of the diethylamino group, and the decay time, τ, depends on solvent viscosity, ν, as $\tau \propto \nu^{2/3}$.[29,35] On the basis of this model, we could interpret the size dependence of RB to the higher viscosity in the nanometer-sized channels, which was consistent with the consideration on the nanometer-sized channel fluidics in the former section. The umbrella-like motion (ULM) model[29,33] is another model for the deactivation of RB. In this model, the internal conversion from the lowest excited state to the ground state is governed by ULM of the amino group from a planar to a pyramidal structure, which causes charge transfer from the amino group to the xanthene ring. When the carboxyl group is solvated strongly, the interaction between the xanthene ring and carboxyphenyl group decreases, and the decay time becomes shorter. Therefore, the decay time becomes longer with a decrease in solvent polarity. On the basis of this model, we attributed the size dependence of RB to lower solvent polarity in the nanometer-sized channels, which would be analogous to the consideration for R6G and SR101.

The time-resolved fluorescence measurements suggested that an aqueous solution in the nanometer-sized channels had a lower dielectric constant (polarity) and higher viscosity. These effects may be due to interactions between the surface charge of the fused-silica and the hydrogen-bond network. In 1980, Stanley and Teixeira[36] proposed a percolation model for a statistical thermodynamic explanation of the hydrogen-bond network of liquid water. When our experiments are described with the model, the water in the nanometer-sized channels can be regarded as space-limited 4-site particles with high-density hydrogen-bond starting or terminating points on the channel wall. The collective hydrogen-bond state of the water in the nanometer-sized channels is possibly enhanced, as compared with that of bulk water. The enhancement of the hydrogen-bond network can be considered as a quasisolid state of the water, and it affects macroscopic parameters, such as viscosity and dielectric constant. Although the liquid properties in the nanometer-sized channels should be investigated by various kinds of experiments, such as surface modification, the results we presented in this study indicated at the very least a difference between the bulk and nanometer-sized liquid. We have presented the interrelation between the liquid and wall properties in nanometer-sized channels, including chemical reactions, as an open problem.

CONCLUSIONS

We have fabricated nanometer-sized channels and demonstrated a liquid introduction method into the channels utilizing capillary action. The video image of the liquid introduction was analyzed by capillarity and hydrodynamics. In addition, liquid properties in the nanometer-sized channels were investigated by time-resolved fluorescence measurements of aqueous solutions of R6G, SR101 and RB. The results suggested that the aqueous solutions in the nanometer-sized channels have lower dielectric constants (polarity) and higher viscosities. To confirm the size effect, further experiments on liquid properties, such as measurement of dielectric constant, low-frequency Raman scattering spectroscopy, and flow visualization, should be performed. From the viewpoint of analytical applications of the nanometer-sized channels, we will also investigate pressure-driven and electrophoretic flows in them.

ACKNOWLEDGMENT

We acknowledge Dr. Yasuhiko Sugii and Prof. Koji Okamoto of Nuclear Engineering Research Laboratory, University of Tokyo, for their support in video analysis with the high-speed camera. We gratefully acknowledge Kiyoshi Sato, Kenichiro Hashimoto, and Yoshio Murai of University of Tokyo for their technical contributions. This research was supported in part by the Ministry of Education, Science, Sports, Culture and Technology of Japan, Grant-in-Aid for Scientific Research on Priority Areas (A), 12042218, 2000 for Scientific Research on Priority Area (B), 13124203, 2001, and for Encouragement of Young Scientists, 14750600, 2002.

Received for review May 28, 2002. Accepted October 2, 2002.

AC025808B

(34) Casey, K. G.; Quitevis, E. L. *J. Phys. Chem.* **1988**, *92*, 6590−6594.
(35) Tredwell, C. J.; Osborne, A. D. *J. Chem. Soc., Faraday II* **1980**, *76*, 1627−1637.
(36) Stanley, H. E.; Teixeira, J. *J. Chem. Phys.* **1980**, *73*, 3404−3422.